Tribology International 219 (2026) 111861

Contents lists available at ScienceDirect

Tribology International

journal homepage: www.elsevier.com/locate/triboint

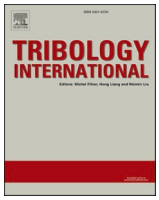

Plain and fretting fatigue experimental test with inconel 718 at room and high temperature

María Moreno-Rubio [a,*], Jesús Vázquez [b], Carlos Navarro [b], Jaime Domínguez [b]

[a] Universidad de Huelva, Escuela Técnica Superior de Ingeniería, Departamento de Ingeniería Minera, Mecánica, Energética y de la Construcción, Campus el Carmen s/n, C.P., 21007, Spain
[b] Universidad de Sevilla, Escuela Técnica Superior de Ingenieros, Departamento de Ingeniería Mecánica y Fabricación, Camino de los Descubrimientos s/n, C.P., 41092, Spain

ARTICLE INFO

Keywords:
Fretting fatigue
Inconel 718
High temperature
Fracture surface
Oxide

ABSTRACT

In this study, the fretting fatigue behaviour of Inconel 718 was analysed at both room and high temperature (650°C) using 'dog-bone' fretting fatigue specimens with a cylindrical contact pad. Inconel 718 is a nickel-chromium-based superalloy widely used in the aeronautical industry due to its excellent mechanical properties, including resistance to oxidation and corrosion, even at high temperatures. Additionally, the material was heat-treated to enhance its mechanical performance. Different tests were conducted in the laboratory under various (axial) load levels to analyse the fretting fatigue behaviour of Inconel 718 at both temperatures. To achieve this, fretting fatigue and plain fatigue curves were obtained. In addition, interrupted fretting fatigue tests were carried out to gain a deeper understanding of crack evolution at elevated temperatures. The study was further complemented by an analysis of surface oxidation and the fracture surface of fretting fatigue specimens.

1. Introduction

Fretting fatigue is a surface damage mechanism that appears in mechanical joints subjected to fluctuating contact forces. This phenomenon is common in a wide range of engineering applications, including bolted assemblies, joints, cables, and is especially critical in blade-disc connections of aircraft gas turbines [1–3]. In such situations, micro-scale relative displacements between contact surfaces, combined with friction, generate stress concentrations that lead to premature surface crack initiation and subsequent propagation, potentially resulting in a structural failure [4].

Nickel-based superalloys are extensively used in the aerospace industry due to their high mechanical strength and stability at elevated temperatures. Among them, Inconel 718 (IN718) is widely employed in turbine discs, blades, compressors and combustion chambers, owing to its favourable combination of strength, ductility and damage tolerance under service conditions.

Previous studies have investigated fretting fatigue behaviour in a wide variety of materials. Early research addressed this phenomenon in aluminium alloys, titanium alloys and nickel-based superalloys, highlighting the influence of parameters such as normal load, temperature and friction coefficient on fatigue life [5–10]. In the case of nickel-based superalloys, fretting fatigue tests have been conducted on materials such as IN100 [11], Inconel 600 [12] and Inconel 690 [13], both at room temperature and at elevated temperatures, revealing material-dependent responses associated with their mechanical behaviour at high temperature.

More recently, several authors have focused on Inconel 718 due to its industrial relevance. Almeida et al. [14] investigated the effect of applying a cyclic normal contact load in fretting fatigue tests on IN718, showing that this loading condition can significantly increase fatigue life at both room and elevated temperatures. Wang et al. [15] analysed high-frequency fretting fatigue tests on IN718 and reported a reduction in fatigue life at high temperature, with *S-N* curves that were nearly parallel to those obtained at lower temperatures. In addition, the authors of the present work previously studied the plain fatigue and fretting fatigue behaviour of IN718 at both room temperature and high temperature (650 °C) [16]. That study established *S-N* curves for different axial load levels and demonstrated a significant reduction in fatigue life under fretting conditions compared with plain fatigue. It was also observed that temperature had a particularly strong influence during the crack propagation stage. These observations highlighted the interest in further analysing crack evolution under fretting conditions, especially considering the effect of temperature.

* Corresponding author.
E-mail address: mmorenor@dimme.uhu.es (M. Moreno-Rubio).

https://doi.org/10.1016/j.triboint.2026.111861
Received 28 November 2025; Received in revised form 2 February 2026; Accepted 20 February 2026
Available online 22 February 2026

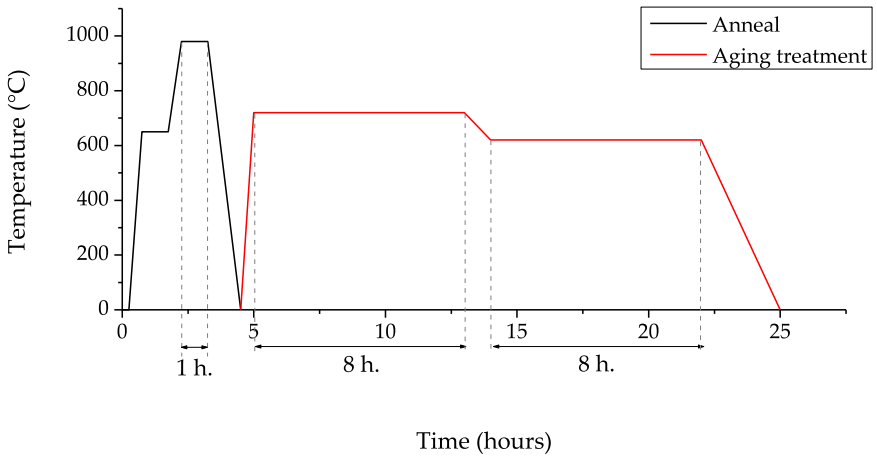

Fig. 1. Heat treatment performed.

The present work aims to extend and deepen the understanding of fretting fatigue behaviour of Inconel 718 at both room and elevated temperatures. To this end, the previous experimental campaign is expanded by incorporating additional plain fatigue tests at high temperature and fretting fatigue tests at room and high temperature, performed under the same normal load conditions that in the previous work, and including an additional normal load level. This allows for an improved definition and reliability of the previously obtained *S-N* curves. Furthermore, interrupted fretting fatigue tests are carried out to investigate crack length evolution with cycles under fretting conditions at high temperature. Finally, a detailed morphological analysis of the fracture surfaces and fretting scars is performed.

In this context, interrupted fatigue tests have been widely used as an effective methodology to analyse crack evolution throughout fatigue life, allowing the mechanisms of crack initiation and the early stages of propagation to be investigated separately. In the field of fretting fatigue, this approach has been employed by several authors to correlate crack length and morphology with defined fractions of the total fatigue life, providing valuable insight into crack propagation under contact conditions. Previous works have shown that controlled interruption of the tests enables characterisation of the initial crack path, its orientation and its evolution as a function of the number of applied cycles, making this methodology particularly suitable for detailed analysis of fretting damage [17–19].

2. Material

As previously mentioned, Inconel 718 will be used for the development of this work. This is a nickel-based superalloy that exhibits high mechanical properties both at room and high temperatures, as well as excellent resistance to oxidation and corrosion. The material is supplied by the company Special Metals, since it is a registered trademark of this company.

In the aeronautical industry, a specific heat treatment is usually required to achieve the high mechanical properties offered by this material. Typically, Special Metals supplies the material in the solution-annealed conditions so that it can subsequently undergo the appropriate heat treatment according to the service conditions. Along with the supplied material, the company provides the possible heat treatment processes required to guarantee the mechanical properties indicated in the technical data sheet. The company also provides a certified material test report for the batch.

The heat treatment followed in this work corresponds to the AMS 5596 and AMS5663 standards, consisting of two stages. The first stage is solution annealing, in which the material is heated to 980 °C for 1 h, followed by rapid cooling with cold air. The second stage corresponds to the hardening process: first, the material is kept at 718 °C for 8 h, then cooled down to 621 °C and held at this temperature for an additional 8 h. Finally, cooling is carried out with nitrogen, completing a total of 18 h of aging. Fig. 1 shows a schematic of the heat treatment process: the black line represents the solution annealing stage, while the red line corresponds to the hardening stage.

Table 1
Mechanical properties [16].

Material properties		Room temperature (Experimentally)	Room Temperature (Technical sheet)	650 °C (Technical sheet)
Tensile strength	σ_u	1435 MPa	1476 MPa	1172 MPa
Yield strength ($R_{P0.2\,\%}$)	σ_y	1310 MPa	1326 MPa	1080 MPa
Young's modulus	E	217 GPa	200 GPa	163 GPa
Poisson's ratio	ν	-	0.294	0.283
Vickers Hardness	Hv	454	435	-

The mechanical properties of IN718 used in the present work were previously characterised and validated by the authors in a former publication [16]. For clarity, the most relevant mechanical properties are summarised in Table 1.

The chemical composition of Inconel 718, as indicated in the datasheet, is presented in Table 2 [16]. As can be observed, nickel, iron, chromium, and niobium are the predominant elements, which is consistent with the typical composition reported in the literature for this alloy [20–23]. The microstructural characteristics and chemical composition of the material have been previously analysed and reported by the authors in an earlier work [16].

The grain size was measured in a previous study [16]. In that study, measurements were taken on two specimens after testing, one at room temperature and other at high temperature, in both longitudinal and transverse directions. In both cases, a longitudinal grain size of 41–42 μm and a transverse grain size of 27 μm were observed. The longitudinal grain size measured is similar to that reported by Yiting Zhan et al. [72], who obtained a value of 36 μm.

3. Procedures of experimental test

In this investigation, two main testing methods were used: plain fatigue testing and fretting fatigue testing. To consider thermal effects, both methods were conducted at room temperature and at an elevated temperature of 650 °C, as mentioned before. Additional experiments were also carried out, including interrupted tests and evaluations of the friction coefficient.

Table 2
Chemical compositions of Inconel 718 alloy (wt%) [16].

C	Mn	Fe	S	Si	Cu	Ni	Cr	Al	Ti
0.03	0.11	18.02	0.0004	0.7	0.13	53.52	18.23	0.47	1.03
Co	Mo	Nb	Ta	B	Bi	P	Pb	Se	
0.13	3.01	5.18	0.004	0.002	0.000001	0.008	0.00003	< 0.000001	

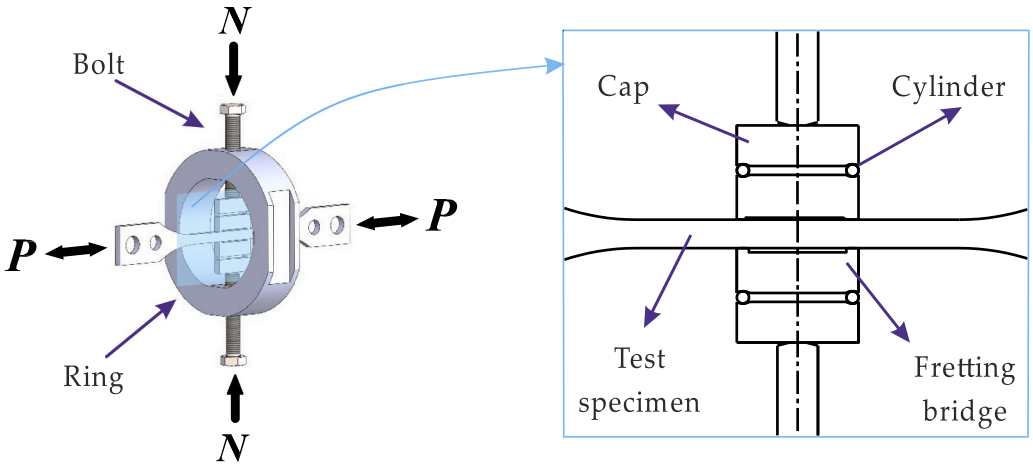

Fig. 2. Scheme of fretting fatigue device (with HT test specimen).

3.1. Plain fatigue test

The geometry of the plain fatigue specimens and the detailed testing procedure have been described in a previous publication by the authors [16]. In brief, the plain fatigue specimens were flat with a minimum cross-sectional area of 7 × 5 mm and a constant radius of 60 mm between their ends. All tests were conducted using a 100 kN capacity MTS servo-hydraulic machine. For high temperature experiments, a commercial furnace was used.

Tests were performed at room temperature (RT) using stress ratios of $R = 0.1$ and $R = -1$. However, because the extension components made the assembly slenderer, high temperature (HT) tests were only conducted at a stress ratio of $R = 0.1$. The frequency was 10 Hz for all tests.

3.2. Fretting fatigue test

The fretting fatigue specimens were dog-bone type geometry, with dimensions of 7 mm in width and 5 mm in thickness This configuration matches that of the plain fatigue test specimens, allowing for a direct and easily comparable results between these two type of test. Similar to the HT plain fatigue test specimens, the HT fretting fatigue test were performed using a commercial furnace.

All fretting fatigue experiments were conducted using a fretting bridge device, a configuration widely adopted and standardised by the Japan Society of Mechanical Engineers [24]. The detailed geometry of the device and the general testing procedure have been previously reported by the authors [16] and therefore not repeated here. Even so, it is important to know that in this setup, a constant normal load is applied through the fretting bridge, while a cyclic axial load is imposed on the specimen via a servo-hydraulic machine. The contact between the fretting bridge and the specimen is of cylindrical type. A schematic representation of this setup is provided in Fig. 2.

Additionally, the tangential load was measured in fretting fatigue tests at RT. This was made possible by placing strain gauges on the fretting bridge, which, under a previous calibration, allow to measure the tangential force during cyclic loading. Since a new set of fretting bridges is used for each test, a new calibration must be carried out before starting a test. The calibration process is identical to the standard

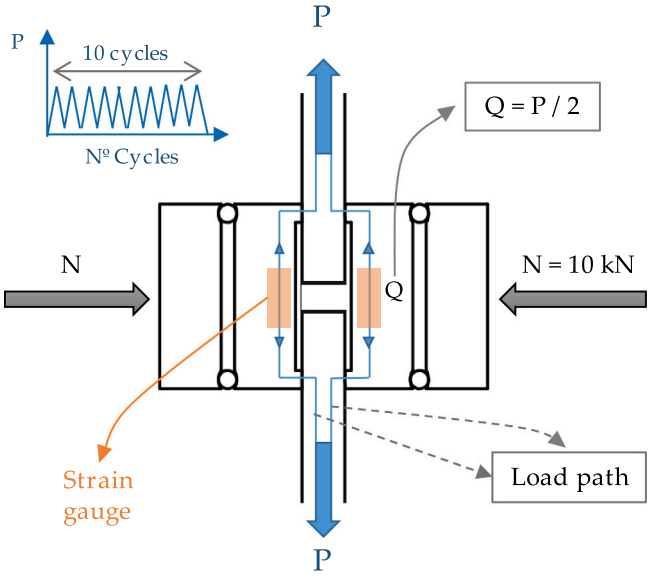

Fig. 3. Scheme of fretting fatigue calibration.

fretting fatigue test, with one notable exception: the calibration is performed on an ad hoc sample that has been cut in half. This guarantees that the total axial load applied by the actuator is effectively transferred via the fretting bridge. Fig. 3 depicts the route by the axial force through this configuration. This illustrates that axial force is assumed to be equally distributed between the two bridges. This means that the tangential load generated by each bridge is half of the applied axial load. To verify the calibration of the bridge, ten load cycles were applied. An HBM Quantum X acquisition system was used to record the normal and tangential loads.

Plain fatigue tests were initially conducted at a frequency of 10 Hz. The same frequency was subsequently considered for the fretting fatigue tests; however, during preliminary fretting fatigue tests, small dynamic effects such as vibrations and instability of the fretting device were

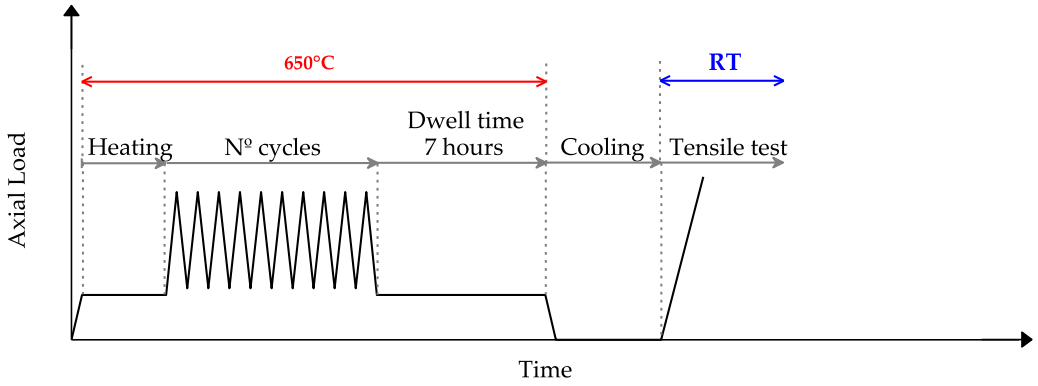

Fig. 4. Fretting fatigue interrupted test of type 1 - FFI-1.

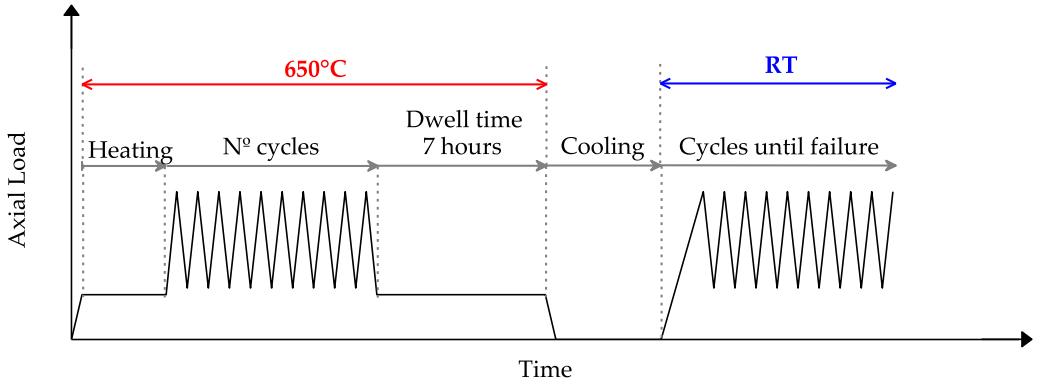

Fig. 5. Fretting fatigue interrupted test of type 2 - FFI-2.

observed at this frequency. For this reason, the loading frequency in fretting fatigue tests was reduced to 8 Hz to ensure stable test conditions. Nevertheless, similar fatigue behaviour is expected between 10 and 8 Hz. Previous studies have shown that, in plain fatigue tests, variations in loading frequency within this range do not lead to significant differences in fatigue response [25].

3.3. *Fretting fatigue interrupted test*

The main aim of interrupted tests is to investigate the fatigue crack evolution. In these tests, the crack's length is examined after a predetermined number of cycles. It should be emphasised that this part of the study was assessed exclusively under HT fretting fatigue conditions, given the limited amount of available literature on such cases.

These tests are conducted using the same apparatus, tools, and methodology as those mentioned in the previous section "Fretting fatigue test." The main distinction is that these tests are not carried out to complete fracture of the specimen under continuous cyclic loading. Instead, its duration depends on the specific type of interrupted test used, which will be detailed below.

In total three different kinds of interrupted tests were conducted:

a) First type of interrupted test: FFI-1.

Following a certain number of cycles, the test stops and the specimen is placed in a furnace operating at 650 °C for seven hours while subjected to a 100 N load. This causes surface crack oxidation, which makes visible the fatigue crack surface. After that, the furnace is turned off, and the system as a whole is left to cool. The apparatus is then disassembled, and a tensile test, in which the axial load is gradually increased until the specimen fractures, is used to rupture it. Fig. 4 shows a schematic of this procedure.

Occasionally, the crack may be too small to result in a brittle

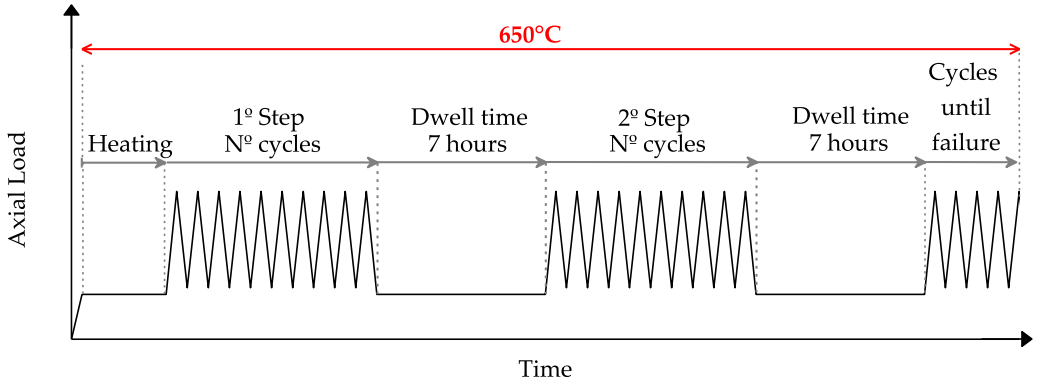

Fig. 6. Fretting fatigue interrupted test of type 3 - FFI-3.

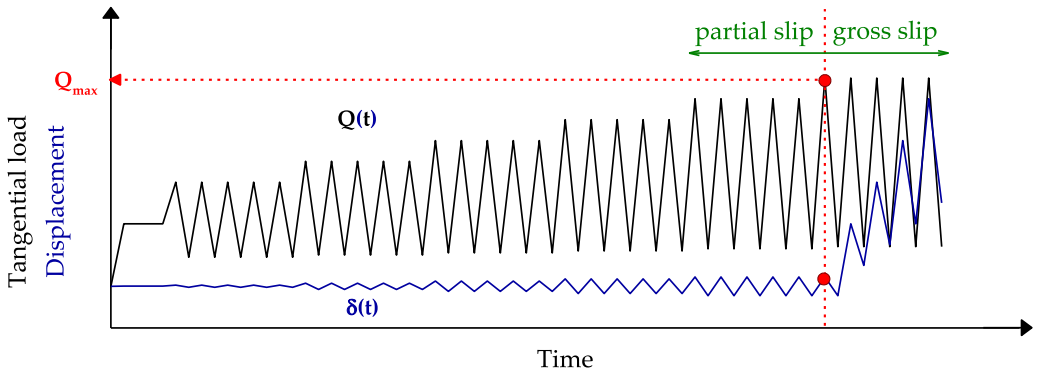

Fig. 7. Scheme of friction coefficient test.

fracture when a tensile test is performed following an interrupted test with a very small number of cycles, making crack measurement impossible. This leads to the second kind of interrupted test.

b) Second type of interrupted test: FFI-2.

This test follows the same process as the first type (FFI-1): the specimen is subjected to fretting fatigue for a predefined number of cycles and then allowed to dwell in the furnace at HT for seven hours. The main difference is that the setup remains intact after cooling and then a fretting fatigue test is conducted at RT until failure to ensure the specimen fails due to a fretting crack initiated in the contact area. It should be noted that oxidation takes place during the furnace dwell time at HT, which makes it possible to measure the fracture length. Fig. 5 shows a schematic of this procedure.

c) Third type of interrupted test: FFI-3.

The purpose of this test was to develop a more effective interrupted test technique that would enable the observe fatigue crack length evolution in a single test. This was achieved by using oxidation caused by several interruptions and the related dwell times without cycles. This kind of interrupted test involves cycling the specimen a certain number of cycles, followed by a 7 h' period at high temperature, after which the cycle loading begins again. This procedure is carried out as many times as needed. The basic idea is to conduct a continuous test at high temperatures with the same load level until the component fails. Fig. 6 shows a schematic of this procedure.

3.4. Friction coefficient test

The friction coefficient is determined by conducting a fretting fatigue test under partial slip conditions. In this test, an ad hoc test specimen cut in half is employed, an essential step to ensure that all the axial stress is passed via the fretting bridge, thus matching the tangential load generated in the fretting bridge, Q, to half of the supplied axial load, σ (i.e., $Q = P/2$). Again, the scheme shown in Fig. 3 can be used to represent the load path under this configuration. The whole normal load of 10 kN is divided into the two contact pads of each fretting bridge, as shown here, with $N_{pad} = N/2$.

This test involves gradually increasing the axial cyclic load amplitude, which results in an increase in the tangential load amplitude throughout the test. The friction coefficient is known to grow in the slip zone during the first cycles of the test before stabilising [26,27]. As a result, increasing the loading amplitude must be done with precaution to make sure global sliding does not occur, damaging and displacing the contact zone before the stabilized friction coefficient is achieved throughout the contact zone.

Although the test is performed under load control, displacement limits are imposed in the test control program to ensure the stability of the experimental setup. These limits prevent a complete disengagement of the half-specimens from the fretting bridge once gross slip is reached. Moreover, since the applied axial load is cyclic rather than monotonic, the measured displacement does not increase monotonically. Instead, the displacement evolves in a cyclic manner, exhibiting local oscillations associated with the minimum/maximum load level of each cycle, while progressively increasing from cycle to cycle.

Initially, the test operates in the partial slip regime, which means that just a fraction of the contact area slips. As Q increases, so does the slip contact zone, but at the same time the friction coefficient increases with the number of cycles decreasing the slip zone. As the displacement amplitude gradually increases, the system remains in the partial slip regime, indicating that $Q < \mu N_{pad}$. This process continues until the slip zone covers the whole contact zone and the friction coefficient has reached its limit. At this moment the displacement rapidly increases, indicating the transition from partial slip to gross slip. The greatest tangential load in the test occurs right before the transition, as defined by the equation $\mu = Q_{max}/N_{pad}$. Fig. 7 depicts a schematic of this method.

As this process develops, the normal load remains constant, just like in the experimental fretting fatigue test. Following the described procedure, four tests were performed, one at RT and three at HT, as indicated in Table 3. The mean of the three HT measurements was 0.33.

Table 3
Results of friction coefficient test.

RT	HT
0.43	0.37
-	0.29
-	0.33

4. Results of experimental campaign

4.1. Plain fatigue and fretting fatigue results

This section shows results from plain and fretting fatigue test at RT and HT (650 °C). The results obtained from plain fatigue test at RT were previously reported and discussed in detail by the authors in [16].

In the previous study, plain fatigue tests were performed in two batches: a first batch with a stress ratio of $R = -1$, and a second batch with a stress ratio of $R = 0.1$. The main reason for this change in stress ratio was that the fretting fatigue and high temperature tests could not be performed with a stress ratio of $R = -1$, as explained in the previous section. This was due to vibrations and uncontrolled movements in the fretting ring during the test and the use of an extension piece at high temperature. Using the Goodman's criterion, good agreement between the different stress ratios was demonstrated, allowing direct comparison between the different type of tests. A total of six different axial loads were selected for the first batch, some of which were repeated, making a total of sixteen tests with $R = -1$. In this case the fatigue limit (amplitude) was found to be 500 MPa. Under the second condition, $R = 0.1$, only three tests were performed to verify the equivalence obtained using

Table 4
Fretting fatigue test results at RT.

Nº Test	σ_{max} (MPa)	N (kN) theoretical	N (kN) measured	Q_{min} (kN) measured	Q_{max} (kN) measured	N_f (Cycles)
FF-RT(1)-1	1100	10	10.06	-1.99	2.07	17136
FF-RT(1)-2*	900	10	9.78	-1.79	1.70	33225
FF-RT(1)-3*	650	10	9.76	-1.21	1.24	117619
FF-RT(1)-4*	650	10	9.45	-0.87	1.56	108770
FF-RT(1)-5*	575	10	10.03	-0.82	1.33	196902
FF-RT(1)-6*	450	10	10.03	-0.83	0.89	431624
FF-RT(1)-7*	400	10	9.91	-0.56	0.99	648348
FF-RT(1)-8*	350	10	10.03	-0.13	1.22	900000
FF-RT(1)-9*	320	10	9.92	-0.13	1.02	1.05E+ 06
FF-RT(1)-10*	320	10	9.80	-0.24	0.95	1.21E+ 06
FF-RT(1)-11*	275	10	10.05	0.08	1.20	2.83E+ 06
FF-RT(1)-12	240	10	10.18	-0.10	0.84	5.00E+ 06
FF-RT(2)-1	900	7	6.93	-1.60	1.65	28048
FF-RT(2)-2	700	7	6.88	-1.32	1.17	69158
FF-RT(2)-3	700	7	6.98	-1.36	1.17	74149
FF-RT(2)-4	400	7	7.09	-0.62	0.84	702049
FF-RT(2)-5	275	7	7.00	-0.09	1.00	1.88E+ 06

* indicates those results that were already reported in [16].

the Goodman stress.

The RT plain fatigue tests were compared with the literature, showing good agreement, as was previously demonstrated by the same authors in [16]. In that article, an additional analysis of the mean stress effect was carried out using SWT parameter, providing a consistent approach to the accounting of these effects.

In the case of the plain fatigue tests conducted at HT, most of the experimental data were also previously reported in [16] and are therefore not reproduced here, corresponding to six tests over a range of axial stresses from 831 MPa to 1094 MPa. However, one additional HT plain fatigue test was performed in the present study. This test was conducted at 650 °C with a stress ratio of $R = 0.1$, a loading frequency of 10 Hz, and a maximum axial stress of 1000 MPa, resulting in a fatigue life of 9857 cycles. This result is consistent with the HT plain fatigue data reported in the previous publication.

In the case of fretting fatigue tests two different normal loads were used: 10 and 7 kN. The selection of these normal loads was based on a preliminary finite element study performed using ANSYS, with the objective of identifying the minimum normal load that ensures partial slip conditions and prevents the occurrence of gross sliding. It is convenient to remember that this load is shared between two contacts, i.e. each contact sees half this value. In both cases, the frequency was 8 Hz and $R = 0.1$. In the fretting fatigue tests at room temperature, the normal load and tangential load could be measured throughout the test. This was possible thanks to the installation of strain gauges and the use of a data acquisition system called Quantum X. Therefore, Table 4 shows the following values: σ_{max}, theoretical normal load, measured normal load, measured tangential load (Q) and cycles to failure. First, there is a batch in which the tests were carried out with a normal load of 10 kN. In this case, 10 tests were performed with different axial loads, repeating two of them (650 and 320 MPa), making a total of 12 tests. In this case, the fatigue limit was reached with a maximum axial load of 240 MPa. Next, for a normal load of 7 kN, a total of five tests were done, of which only the axial load of 700 MPa was repeated.

Finally, HT fretting fatigue tests were performed under the same normal load conditions (10 and 7 kN), $R = 0.1$ and a frequency of 8 Hz. The difference between HT and RT fretting fatigue tests is that it was not possible to measure the normal and tangential loads throughout the entire duration of the test. In this case, only the normal load could be measured before the test was executed. Under the first normal load of 10 kN, tests were performed with 9 axial load levels, making a total of 16 tests. A series of tests were conducted to determine whether extending the preheating time prior to loading had an impact on the specimen lifetime. It was expected that specimens subjected to higher loads, and consequently shorter test durations, would be more sensitive to variations in preheating time, since this period constituted a greater

Table 5
Fretting fatigue test results at HT.

Nº Test	σ_{max} (MPa)	N (kN) theoretical	HTO (Hours)	$N_{f\text{-}H}$ (Hours)	N_f (Cycles)
FF-HT (1)-1	1100	10	1	0.10	2960
FF-HT (1)-2	1100	10	2.5	0.10	2796
FF-HT (1)-3*	900	10	1	0.30	8502
FF-HT (1)-4	900	10	2.5	0.26	7525
FF-HT (1)-5	750	10	1	0.60	17321
FF-HT (1)-6	750	10	2.5	0.51	14766
FF-HT (1)-7	750	10	16.5	0.51	14812
FF-HT (1)-8	750	10	2	0.44	12678
FF-HT (1)-9	750	10	2	0.46	13138
FF-HT (1)-10*	650	10	1	0.91	26173
FF-HT (1)-11	575	10	1	1.13	32564
FF-HT (1)-12*	500	10	1	1.86	53556
FF-HT (1)-13	450	10	1	3.84	110680
FF-HT (1)-14*	400	10	1	5.77	166148
FF-HT (1)-15	350	10	1	149.31	4.30E+ 06
FF-HT (1)-16	350	10	1	173.61	5.00E+ 06
FF-HT (2)-1	700	7	1	0.63	18276
FF-HT (2)-2	575	7	1	1.03	29767
FF-HT (2)-3	450	7	1	3.68	106095
FF-HT (2)-4	400	7	1	2.91	83766
FF-HT (2)-5	400	7	1	173.61	5.00E+ 06
FF-HT (2)-6	400	7	1	28.19	811930

* indicates those results that were already reported in [16].

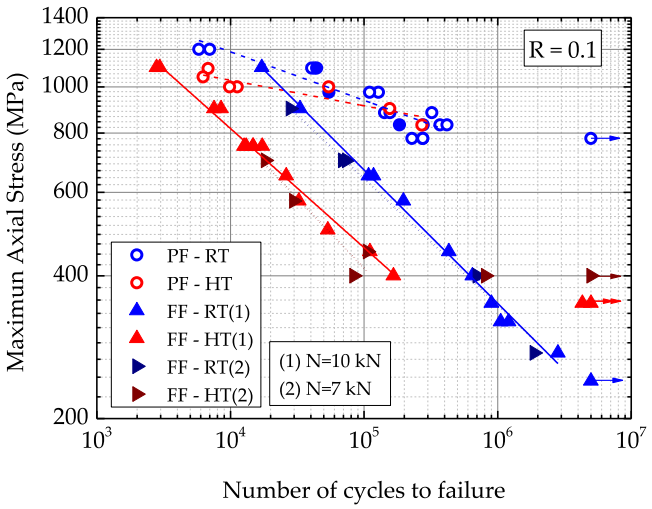

Fig. 8. Plain and fretting fatigue test at RT and HT (650 °C).

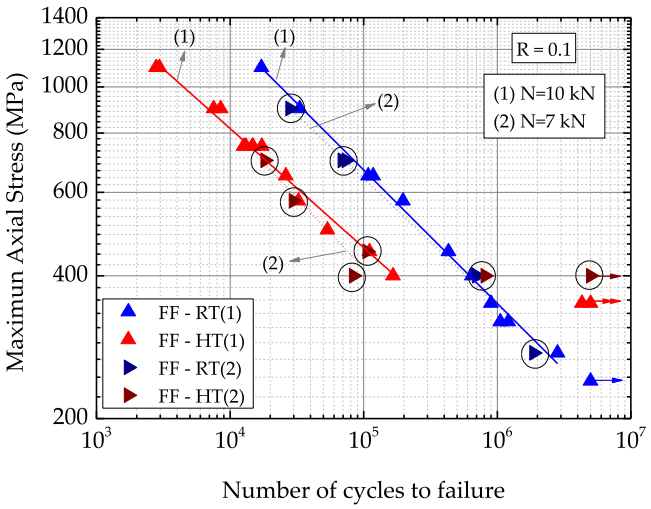

Fig. 9. Fretting fatigue test at RT and HT (650 °C)., with normal load of 10 kN and 7 kN.

proportion of their overall thermal exposure compared to low load, long duration tests. Table 5 presents σ_{max}, *N*, HTO (the heating time inside the furnace before start-up), and the lifetime in hours and cycles.

As a consequence, the first preheating time was extended from 1 h to 2.5 h, and the tests performed at 1100, 900, and 750 MPa were repeated. With the exception of the 750 MPa axial load, this first change showed that while the lifespan did reduce, the reduction was not substantial. In order to determine whether the observed variations in 750 MPa were caused by the preheating period or the inherent variability of experimental testing, three more experiments were carried out at this axial load (750 MPa) with different preheating times of 16.5 h and 2 h. The findings clearly demonstrated that preheating for up to 16.5 h had no negative impact on fatigue life. For instance, the 750 MPa tests involving two hours of preheating had a shorter fatigue life than those involving 2.5 or 16.5 h.

In these tests, the fatigue limit was found to be 350 MPa. Two tests were performed at this axial load level; however, one of these had to be stopped after 4.3 million cycles due to a servo-hydraulic machine issue. Nevertheless, the authors consider that this was close to the established run out of 5 million cycles. Accordingly, the test was repeated, verifying that 5 million cycles were reached and thus confirming the fatigue limit.

For the series conducted under a normal load of 7 kN, six tests were carried out across four distinct axial stress levels, with the lowest level of 400 MPa being tested in duplicate. Among the three specimens evaluated at this stress level, one exhibited infinite life, thereby identifying 400 MPa as the fatigue limit.

The fatigue life results obtained from the different types of tests (plain fatigue and fretting fatigue) are shown by their *S-N* curves in Fig. 8. Plain fatigue tests are shown with circles and are marked with PF in the legend. Fretting fatigue tests are shown with triangles and labelled FF. The colours indicate the test temperature: blue for those performed at room temperature (RT) and red for high temperature (HT, 650 °C). In low-temperature plain fatigue tests, there are two types of circles: solid and hollow. The solid blue circles represent tests performed with $R = 0.1$, while the hollow blue circles show plain fatigue tests at low temperature performed with $R = -1$ and converted with Goodman's ratio to their equivalent in $R = 0.1$.

The graph shows how fretting fatigue life (N_f^{FF}) reveal a shorter lifespan compared to plain fatigue life (N_f^{PF}) at both temperatures. While similar trends were previously suggested by the authors [16], the present study significantly extends the experimental database, allowing these observations to be confirmed with a larger number of fretting fatigue tests and additional testing conditions. This is mainly due to the fact that the contact caused by the fretting bridge in the test piece acts as a stress concentrator [28]. This same behaviour has been observed in the vast majority of materials [12,13]. It is noticeable how the ratio N_f^{FF}/N_f^{PF} decreases quickly as the axial load decreases. This suggests that fretting fatigue damage dominates plain fatigue damage at the high cycle fatigue regime. Furthermore, it is evident that the fatigue life under plain fatigue and fretting fatigue conditions is very similar for large axial loads, approximately 1100 MPa. This suggests that, at these load levels, stress concentration resulting from the mechanical contact does not significantly impact fatigue. This behavior, previously hypothesized by the authors [16], is here experimentally validated through additional fretting fatigue tests conducted at high axial stress levels.

Moreover, the influence of temperature on each testing condition must be considered. Notably, the plain fatigue lives at both temperatures were found to be similar. Temperature effects became significant only for lifetimes shorter than approximately 10^5 cycles. A comparable trend was observed by Kawagoishi et al. [29], who reported similar behaviour in plain fatigue tests conducted at different temperatures.

By contrast, for fretting fatigue tests, temperature effects are evident across the entire fatigue regime. This conclusion is supported in the present work by a substantially larger set of HT fretting fatigue tests than previously reported. Although both curves display nearly identical slopes, they differ in offset, with fatigue life at HT being approximately four times shorter than at RT, except at 1100 MPa where it is reduced by a factor of six. This deviation can be attributed to the diminished influence of contact stress concentration under high axial loading. As previously noted, the fatigue limits were determined to be around 240 MPa at RT and 350 MPa at HT.

The reduced fretting fatigue life at high temperature compared with room temperature, in contrast to the similar conditions observed in plain fatigue, is most likely associated with differences in crack growth behaviour. In plain fatigue, a substantial fraction of the total life is typically consumed during crack initiation, whereas in fretting fatigue, the initiation phase is relatively brief and crack propagation tends to dominate the overall failure process. Thus, this hypothesis suggests that temperature does not affect the crack initiation phase, since no clear variation is observed in plain fatigue tests. However, in the case of fretting fatigue, a variation with temperature was observed throughout the entire load range analysed. This would indicate that, since the propagation phase predominates in fretting fatigue and a clear variation with temperature is observed, temperature significantly affects this phase.

We also have investigated the effect of normal load on fretting fatigue tests, as shown in Fig. 9. This analysis includes a new normal load level of 7 kN, not considered in the previous publication, allowing the influence of contact pressure on fretting fatigue behaviour to be directly

Table 6
Crack length of interrupted test - Type 1 and type 2.

Nº Test	Type of the interrupted test	Nº Cycles	1º Crack length (μm)	2º Crack length (μm)
FFI-1–1	1	10000	636	358
FFI-1–2	1	8000	531	191
FFI-1–3	1	4000	150	-
FFI-1–4	1	4000	152	-
FFI-2–1	2	2000	369	-
FFI-2–1	2	2000	386	222

assessed. In this graph, tests with a normal load of $N = 10$ kN are represented by upward triangles (identified as (1)), whereas those with $N = 7$ kN are represented by downward triangles (identified as (2)). Tests with this lower normal load have also been circled for easy identification. This figure shows that the results for both RT and HT situation are very analogous, with no significant changes between them. However, there was a minor difference in the fatigue limit at HT, with the lower normal load providing a slightly higher fatigue limit. The fatigue limit was not investigated at RT.

As previously discussed, for both normal load, a reduction in fretting fatigue life at high temperature was observed when compared with room temperature. This behaviour was analysed by several authors, such as Kwon et al. and Mall et al., who suggested that the results of high temperature experimental tests may be influenced by variations in mechanical properties. In the case of IN100 [11], Mall et al. observed that the mechanical properties increased with temperature until approximately 650 °C, which resulted in longer lives at elevated temperatures. A similar trend was reported in the studies on Inconel 600 and 690 conducted by Kwon [12,13], where the mechanical properties remained nearly unchanged as the temperature increased, until 600 °C and 500 °C respectively, leading to comparable lives. In contrast, the material under investigation in this study, Inconel 718, exhibits a significant variation, with decreases in yield strength, Young's modulus, and ultimate tensile strength, accompanied by a clear reduction in live at HT. A reduction in live at elevated temperature has also been reported by other authors in the literature, for example, [10] and [14].

Several researchers have investigated the generation of a glazing oxide layer in nickel-based superalloys when exposed to high temperatures, which causes a decrease in the friction coefficient and, as a result, affects fretting fatigue behaviour. It is vital to notice that the oxide layer develops during heat treatment too. Some researchers remove this layer before conducting experiments by polishing the surface, allowing the oxide to regenerate at HT. In this research, however, the oxide layer formed during heat treatment was maintained. Based on this procedure, the authors propose that this oxide layer produces similar surface conditions in both RT and HT testing, and that the reduction in fatigue life is mostly attributable to differences in mechanical properties rather than the oxide layer. This interpretation is reinforced in the present study not only by the extended fretting fatigue dataset at HT, but also by the oxide layer analysis presented in Section 5.1.

4.2. *Fretting fatigue interrupted test*

These experiments are used to investigate the crack length and crack initiation morphology as a function of the number of cycles applied under identical conditions, allowing for direct comparison. To evaluate each type of interrupted test, a normal load of 10 kN and a maximum axial load of 750 MPa were applied.

The FFI-1 (first type of interrupted test) was subjected to four tests interrupted at three different number of cycles: 10000, 8000 and 4000

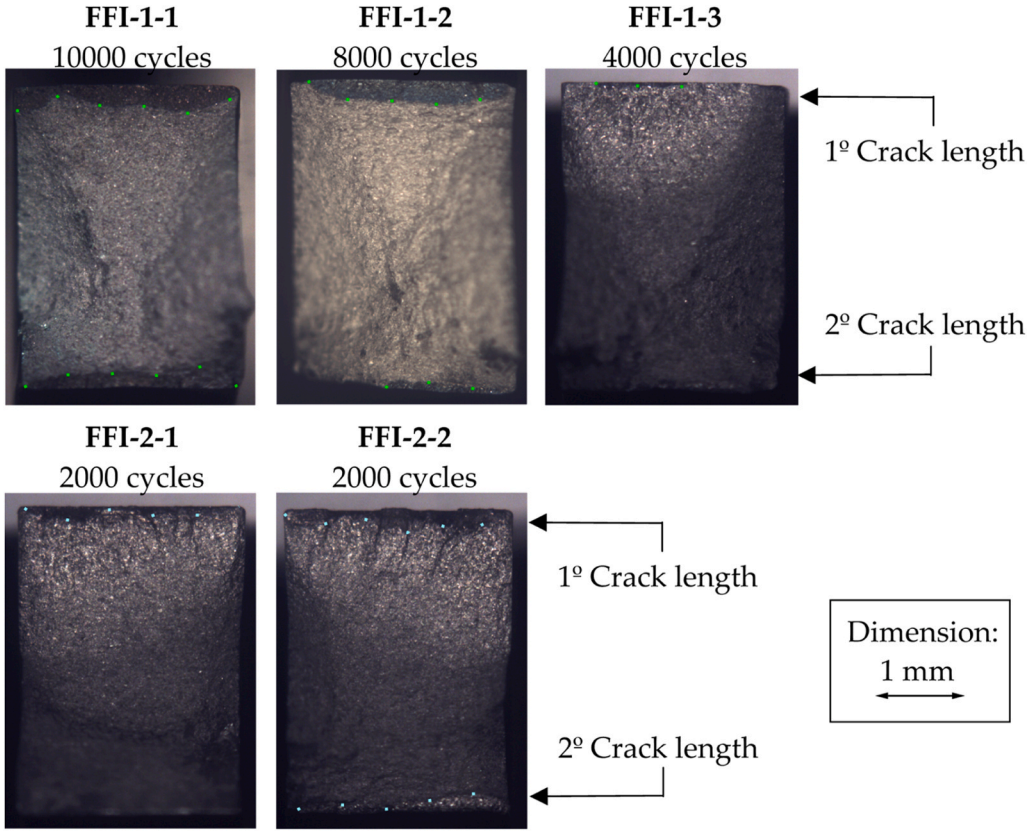

Fig. 10. Interrupted fretting fatigue fracture surface - type 1 and 2.

Table 7
Results of the FFI-3 test.

Nº Test	Step	Step cycles	1º Crack length (μm)	2º Crack length (μm)	Final crack length (μm)	Total life N_f (cycles)
FFI-3–1	1	4000	-	-	2600	11670
	2	8000	505	296		
FFI-3–2	1	4000	-	-	2130	11992
	2	8000	394	290		
FFI-3–3	1	8000	302	253	3065	13553
FFI-3–4	1	8000	270-	-	2480	13232
	2	10000	511	461		
FFI-3–5	1	10000	484	-	2415	12592
FFI-3–6	1	4000	386	222	2345	14249

cycles, with the shortest life test repeated. The measured crack lengths for each test are shown in Table 6. In these experiments, crack growth was clearly detectable, and in some cases cracks developed in two contact regions of the specimen, yielding to two independent crack length measurements for a single test. This behaviour arises from the four contact zones generated by the fretting bridges. The measurements revealed a progressive increase in crack length, varying between 150 μm and 636 μm.

Fig. 10 depicts the fracture surfaces for the three number of cycles investigated. In these experiments, the crack appears much darker than the ductile fracture zone. This difference is due to oxidation that occurs not only during the test but also during the time the specimen remains in the furnace after the cycling has finished.

The results of the FFI-2 (second type of interrupted test) are shown in Table 6. This type of the test was only used for the shortest tests, interrupted at 2000 cycles. As previously said, these type of tests continued cycling at RT with the full setup rather than subjecting the specimen undergoing a tensile test. In this type of tests, one of the most important issues to overcome is how to discern between crack length established during HT cycling and subsequent crack growth at RT. To distinguish between these two crack formation phases, the oxidised area of the specimen is examined. This oxidized region appears darker, similar to FFI-1, whereas the fracture propagation at RT appears lighter grey. Fig. 10 depicts fracture surface images from the two tests undertaken.

FFI-2 resulted in longer crack lengths after 2000 cycles than those measured after 4000 cycles in FFI-1. The reason for this difference is the specific testing methodology used. In particular, the application of tensile loading during the test may cause specimen elongation and influence the final measured crack length. The analysis takes both FFI-1 and FFI-2 into account, and the observed difference is recognised as a methodological effect rather than an inconsistency in the data.

The images from the interrupted tests show how the crack begins as a semi-elliptical shape, but then quickly changes into a through thickness crack.

Up to this point, in FFI-1 and FFI-2, the specimen was cooled after the dwell period and subsequently tested to failure at RT. In contrast, FFI-3 was conducted differently: once the dwell period concluded, the test continued under the same thermal conditions, 650 °C, until specimen failure.

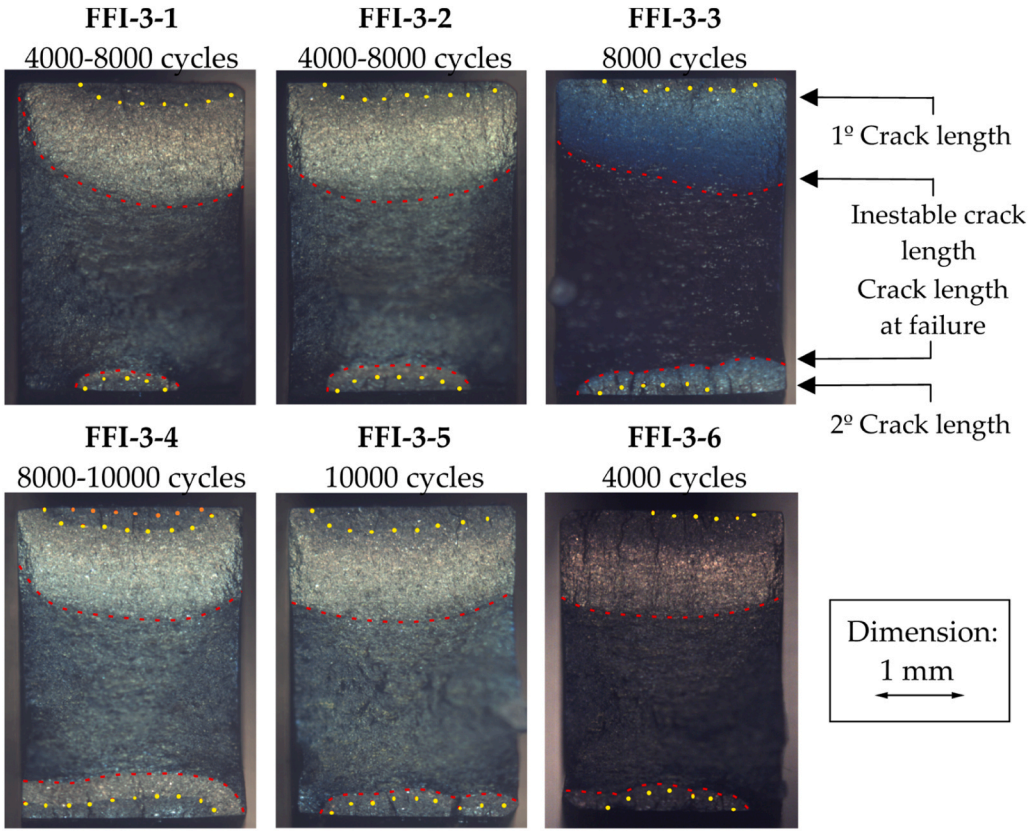

Fig. 11. Fracture surface of marked fretting fatigue test at HT - type 3.

Table 8
Results of final crack length and total fatigue life of FF-HT(1) test.

N° Test	Length to unstable crack (μm)	N_f (cycles)
FF-HT(1)-5	No data	17321
FF-HT(1)-6	2116	14766
FF-HT(1)-7	2448	14812
FF-HT(1)-8	2748	12678
FF-HT(1)-9	2592	13138

Earlier observations indicated that longer exposure within the furnace promoted greater oxidation on the fracture surface, which was visually identified by changes in crack surface coloration. Building on this premise, two dwell periods of 7 h each were incorporated at different fatigue life stages within the same test, allowing two distinct crack lengths to be examined during a single experiment. The first two experiments incorporated two dwell periods of 7 h each, applied at 4000 and 8000 cycles. In both cases, a single distinct transition was detected in the primary crack zone, the crack responsible for specimen failure, measuring 505 μm in the first test and 394 μm in the second. These results suggested that the visible transition was associated with the second interruption at 8000 cycles. To verify this assumption, a third experiment was performed with a single dwell at 8000 cycles, which produced a crack length of 302 μm. From these observations, it can be preliminarily concluded that the transitions correspond to the second dwell at 8000 cycles, with no detectable evidence of the earlier interruption at 4000 cycles.

In the fourth experiment, two interruptions were again introduced, this time at 8000 and 10000 cycles. Examination of the fracture surface revealed a distinct transition at a length of 511 μm, attributed to the crack formed at 10000 cycles. A second, less pronounced transition was also noticeable at a length of 270 μm, which was presumed to correspond to the interruption at 8000 cycles. However, this interpretation could not be confirmed with certainty, as the colour contrast between the two regions was minimal compared with the earlier case. To complete the evaluation of this method, two additional tests were conducted, each with a single interruption: one at 10000 cycles, which produced a crack length of 484 μm, and another at 4000 cycles, with a crack length of 386 μm. These final experiments served to compare and validate the results obtained from the previous tests.

The FFI-3 test results are shown in Table 7. These include the test number, the number of interruptions, the number of cycles at which the interruptions occurred, the length of the main crack (the crack that caused the specimen to fail), the length of the secondary crack, the length of the final crack, and the total number of cycles. Fig. 11 displays these fracture surfaces.

It is evident that crack lengths at various fatigue life values do not differ much. Furthermore, since only one of the two expected crack lengths was apparent in the tests conducted with two interruptions, it can be said that the main goal of this testing model, interrupted fretting fatigue test type 3, needs more research.

Furthermore, this kind of test yields a total fatigue life value and a final crack length, which can be compared with values obtained from uninterrupted tests. The fatigue life and final crack length data for specimens tested uninterrupted at high temperatures with an axial load of 750 MPa and a normal load of 10 kN are shown in Table 8.

Fig. 12 compares the fatigue life from FFI-3 with that of FF-HT(1), which was obtained from fretting fatigue tests without interruptions. In this figure, the black triangles represent the FFI-3 tests; hollow triangles represent tests with a single interruption; and solid triangles represent tests with two interruptions. The red triangles represent the FF-HT(1) tests.

This representation enables the evaluation of fatigue life as a function of the number of interruptions, allowing assessment of whether these pauses influence performance or have no measurable effect. The results reveal a downward tendency: the average life for uninterrupted tests was 14543 cycles, decreasing to 13464 cycles for tests with one interruption and 12298 cycles for those with two. Although this trend suggests a reduction in fatigue life with an increasing number of interruptions, the limited sample size prevents drawing a definitive conclusion.

Fig. 13 depicts the crack length evolution observed during the interrupted tests discussed earlier. The tests are illustrated by several colours: green for FFI-1, blue for FFI-2, black for FFI-3, and red for tests that are completed without interruptions. In all situations, both primary and secondary fracture lengths are provided, and for the FFI-3, the final

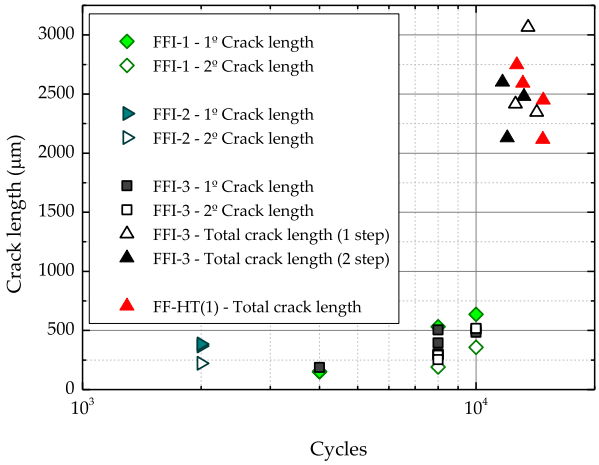

Fig. 13. Fretting fatigue crack evolution at 750 MPa of maximum axial load and 10 kN of normal load at 650 °C.

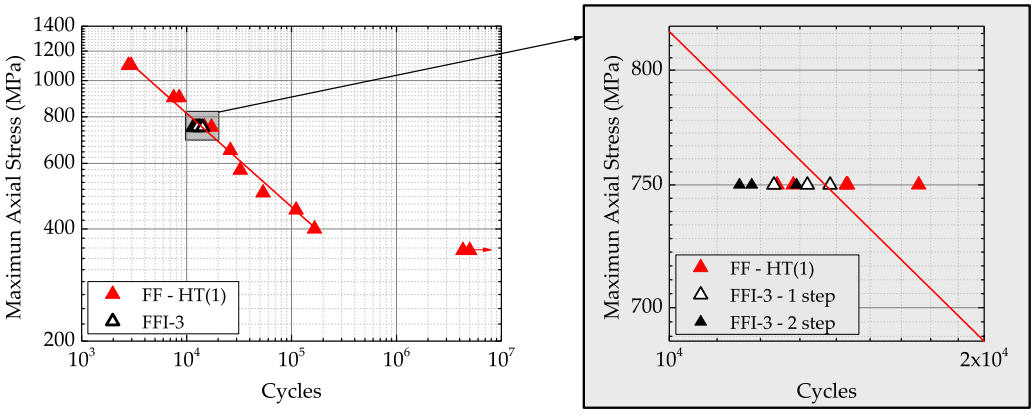

Fig. 12. Fatigue life values of FF-HT(1) and FFI-3 tests at HT.

crack length is presented. There is also a differential between tests with one and two interruptions.

As previously mentioned, the interruptions were performed at specific numbers of cycles. This allowed the crack evolution to be measured at different stages of the test. Observe that the crack length gradually rises with the number of cycles. It is worth mentioning that crack lengths obtained in type 1 tests are comparable to those acquired in type 3 tests. Finally, this figure shows that the number of interruptions has no significant bearing on the final crack length.

5. Fracture surface morphologies

This section analyses the fracture surface resulting from specimens tested under fretting fatigue. A previous study by the same authors [16] observed that the fracture surface was divided into several zones: crack initiation, stable crack growth, unstable crack growth, and a second crack initiation. Additionally, the fracture surface of tests conducted at high temperature exhibited a blue tone, caused by surface oxidation. It was also found that, in the crack initiation and stable crack growth zones, the cracks grew almost perpendicular to the contact surface.

5.1. Composition analysis: oxide layer

It had been said that the fracture surface colour in high temperature tests differs from that in room temperature tests, revealing a variety of blue tones; however, further research has revealed that these tones are not necessarily blue. Observations show that the surface colour can change depending on how long the specimen has been in the furnace after fracture. A blue colour develops when the furnace is switched off immediately after the test is completed, whereas a golden colour appears when the specimen is left in the high temperature furnace for more than six hours after the test is completed, i.e., after fracture.

As a result, the fractures surfaces were examined using Energy Dispersive X-ray Spectroscopy (EDS) in the SEM in order to determine the reason for the colour changes in these surfaces. This analysis was carried out along a straight path along the crack surface beginning at the contact surface and progressing to the final fracture site. It is important to note that this analysis corresponds to a post-mortem characterization of the fracture surface after completion of the fatigue test. The fundamental goal of this analysis is not to determine the chemical composition of the surface, but to investigate the oxidation that has occurred and how it varies in each case, thus this analysis is not intended to establish a direct link between oxidation and fatigue crack propagation during the test. Therefore, just the weight percentage of oxygen on the fracture surface is indicated.

It should be noted that EDS does not probe an infinitesimally thin surface layer, but rather provides an averaged chemical signal over a finite interaction volume beneath the surface. The effective information depth depends on several parameters, including the accelerating voltages, the atomic number, atomic weigh and density of the analysed material.

The electron penetration depth was estimated using Kanaya-Okayama model [30,31], which defines the interaction depth $R_{K\text{-}O}$ as:

$$R_{K-O}(nm) = 27.6 \quad \frac{A\,{E_0}^{1.67}}{Z^{0.89}\,\rho} \tag{1}$$

where A is the atomic weight (g/mol), E_0 is the accelerating voltage (KeV), Z is the atomic number, and ρ is the density of the material (g/cm^3). For the experimental conditions employed in this study, Inconel 718, the values $A = 59.36$ g/mol, $E_0 = 20$ keV, $Z = 27.76$, and $\rho = 8.26$ g/cm^3 were used, resulting in an estimated electron depth is 1.53 μm.

Due to the oxide layer present on the fracture surface is thinner than the estimated EDS interaction depth, the measured oxygen weight percentage cannot be interpreted as an absolute or quantitative value representative solely of the oxide layer. Instead, the oxygen content is used as a qualitative indicator of the presence and relative extent of oxidation on the fracture surface.

Table 9
Summary of the test conditions and cycles for fracture surface analysis.

Nº test	Temperature	N (kN)	σ_{max} (MPa)	N_f (Cycles)	Surface tonality
FF-RT(1)-1	RT	10	1100	17136	Grey
FF-RT(1)-7	RT	10	400	648384	Grey
FF-HT(1)-1	650 °C	10	1100	2960	Blue
FF-HT(1)-14	650 °C	10	400	166148	Blue
FF-HT(2)-3	650 °C	7	450	106095	Golden*

* More than 7 h inside of the furnace at 650 °C after the failure

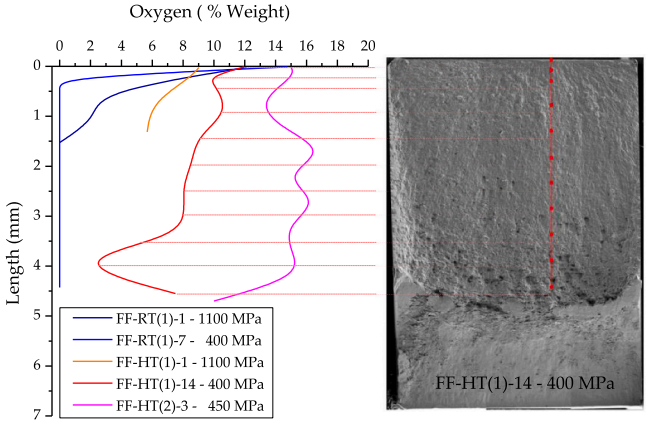

Fig. 14. Oxygen concentration (% weight) on the fracture surface. Image taken at SEM.

Based on numerous literature sources, it might be assumed that increased exposure to high temperatures would result in increased oxide formation. Previous studies by the authors have shown that, for specimens subjected to the same heat treatment, oxygen is confined exclusively to the surface oxide layer, while the underlying bulk material exhibits negligible oxygen content. Consequently, any non-zero oxygen signal detected under identical EDS acquisition conditions can be attributed to surface oxidation, allowing meaningful relative comparisons between specimens with different thermal exposure histories.

Five fracture surfaces were analysed: two from specimens tested at RT and three at HT from tests denoted as FF-RT(1)-1, FF-RT(1)-7, FF-HT(1)-1, FF-HT(1)-14, and FF-HT(2)-3. The Table 9 specifies the characteristics of each test and its subsequent life (this information was previously presented in Section 4). Observing Fig. 14, it is evident that regardless of the test temperature, there is a large proportion of oxygen along the edge of the surface. This oxygen is associated with the oxide layer formed by the aging of the thermal treatment executed, which was not removed as previously stated.

It can be observed that, in the RT tests FF-RT(1)-1 and FF-RT(1)-7, oxidation levels decrease to nearly zero with increasing distance from the contact region. In contrast, the HT tests exhibit a substantial presence of oxygen across the entire fracture surface. For specimens in which the furnace was switched off immediately after fracture (FF-HT(1)-1 and FF-HT(1)-14) the oxygen content shows a slight reduction along the fracture surface, suggesting that regions exposed for a shorter time are less affected, which is consistent with the reduced thermal exposure of these regions.

In contrast, when a specimen is kept at 650 °C for an extended period

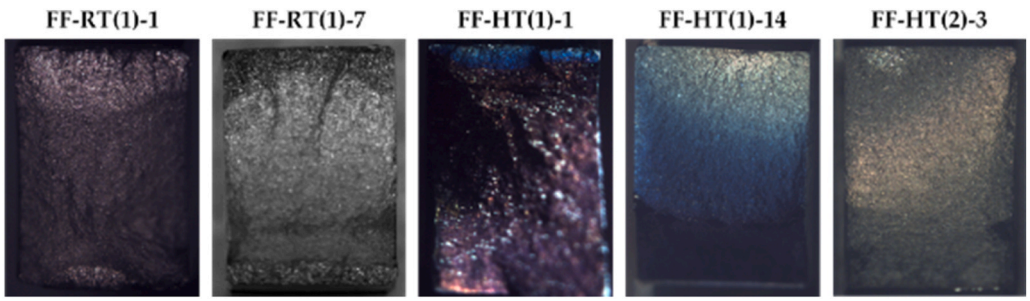

Fig. 15. Photographs of the fracture surfaces of the examined specimens, demonstrating the distinctive tonalities in specimens at RT (grey) and HT (blue and gold).

Table 10
% Oxygen of fracture surface of the test specimens.

RT					HT				
N° Test	σ_{max} (MPa)	%O FCZ	%O SLCZ	%O STCZ	N° Test	σ_{max} (MPa)	%O FCZ	%O SLCZ	%O STCZ
FF-RT(1)-1	1100	15.01	10.4	13.85	FF-HT(1)-1	1100	9.55	14.98	6.72
FF-RT(1)-4	650	12.53	13.75	12.61	FF-HT(1)-10	650	13.33	13.19	12.13
FF-RT(1)-7	400	14.73	14.05	14.83	FF-HT(1)-14	400	14.10	13.6	13.12
Average		14.09	12.73	13.75	Average		12.03	13.92	10.66

after fracture, a substantial amount of oxygen is present, fluctuating within a relatively narrow range. Comparing specimens FF-HT(1)-14 and FF-HT(2)-3, it is evident that, although FF-HT(1)-14 experienced a greater number of cycles, FF-HT(2)-3 (exposed in the furnace for over 7 h after failure) shows a higher oxygen content. This finding suggests that the time of HT exposure is directly related to oxide formation and thus surface coloration. Although EDS does not directly measure oxide thickness, the increasing oxygen signal with longer post-fracture exposure at high temperature is consistent with the development of a thicker oxide layer. Such variations in oxide thickness are known to govern surface colour through optical interference effects, providing a plausible explanation for the observed colour changes. Fig. 15 shows the fracture surfaces of the tested specimens.

As illustrated in Fig. 14, the contact surfaces of all specimens display a considerable presence of oxygen, regardless of whether testing was conducted at RT or at 650 °C, suggesting the existence of an oxide layer under both conditions. In most reports, oxide layer formation is typically associated only with HT exposure. Consequently, the central question at this stage is to determine the origin of oxygen detected in the RT specimens. The main hypothesis, later confirmed through subsequent analyses, is that this oxygen arises from the retained thermal treatment, which was preserved in this study, unlike in most previous works where it was removed after processing by polishing.

Overall, the oxidation features discussed in this section should be interpreted as post-fracture indicators of thermal exposure history and surface condition, rather than as evidence of oxidation-assisted fatigue damage during testing. No attempt is made in this study to identify the specific oxide phases formed; the presence of oxygen is considered solely as an indicator of surface oxidation associated with thermal exposure.

To validate the proposed hypothesis, an EDS analysis was conducted to quantify the oxygen content on the surfaces of six specimens, three tested at RT and three at HT. The measurements were first taken in

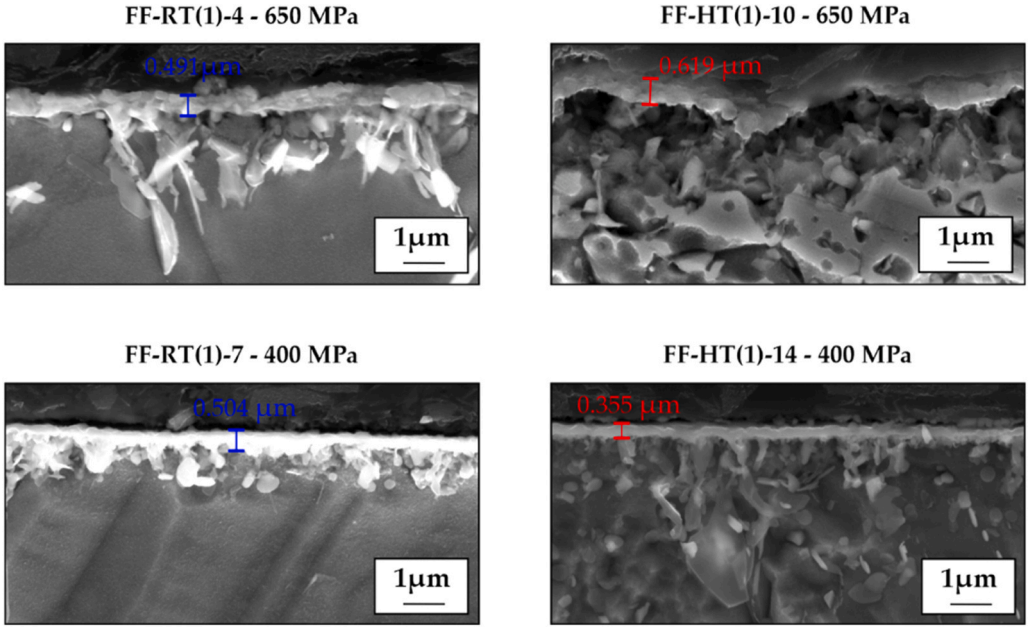

Fig. 16. Oxide layer in FCZ in four test specimens.

Table 11
Thickness of oxide layer in CZ and FCZ.

Test temperature	Contact zone (CZ)	No contact zone (FCZ)
RT	702 nm	632 nm
HT (650 °C)	626 nm	695 nm

regions far from the contact zone (FCZ) to eliminate the influence of fretting fatigue. At both temperatures, specimens tested under different stress levels (1100, 650, and 400 MPa) were examined to encompass a broad range of fatigue lives and, consequently, varying exposure durations in the HT tests. For each specimen, at least two measurements were recorded, except for specimen FF-HT(1)-1, where only one was possible. Table 10 summarises the mean values obtained for each specimen and provides an overall average for each testing temperature.

With the exception of the specimens tested at 1100 MPa, where a value of 15.01 % at RT and 9.55 % at HT was obtained, it is seen that the oxygen values are essentially the same at both low and high temperatures, with the percentage being about 12–15 %, according to the data shown in the Table 10. These findings suggest that a pre-existing oxide layer, which is a result of the heat treatment that was done, is present on all specimens and is comparable among them, with an average at RT of 14.09 % and at HT of 12.03 %.

The same analyses were then carried out in the slip zone (SLCZ) and the stick zone (STCZ), comparing the findings with the unfretted zone (FCZ), in order to assess the impact of fretting contact on the specimen's oxidation. The collected data, both at RT and HT, is shown in Table 10 for each zone. At HT, the average oxygen content in the STCZ is significantly lower than at RT. However, this average is strongly influenced by the result from the 1100 MPa test (FF-HT(1)-1), which shows a notably lower STCZ value of 6.72 %. When examining the 650 MPa and 400 MPa conditions separately, the STCZ oxygen percentages between RT and HT are more comparable (12.61 % vs. 12.13 % at 650 MPa, and 14.83 % vs. 13.12 % at 400 MPa). This suggests that the apparent significant reduction at HT may be driven primarily by the specific conditions or local phenomena.

Another important aspect to consider at this stage is the thickness of the oxide layer and whether it changes with testing temperature or between the analysed regions, namely the FCZ (far from the contact zone) and the CZ (contact zone). To investigate this, the oxide layer thickness was measured in four specimens: FF-RT(1)-4, FF-RT(1)-7, FF-HT(1)-10, and FF-HT(1)-14. Multiple measurements were taken for each specimen at different locations to ensure sufficient data density, with approximately six measurements per zone and specimen. Cross-sectional SEM images of the Inconel 718 specimens, oxidised during the heat treatment and subsequently tested at RT and HT, are presented in Fig. 16. These images illustrate the oxide layer in the FCZ regions. By analysing these areas, unaffected by contact, it becomes possible to assess whether the oxide layer thickness increases or decreases solely as a result of exposure to elevated temperature when a pre-existing layer is already present.

The fracture surface cross-sections of the Fig. 16 were prepared using conventional metallographic procedures and analysed by SEM. Variations in image contrast observed among different micrographs arise from images acquired during different SEM sessions under slightly different imaging conditions, rather than from intrinsic differences in oxide composition or morphology.

Table 11 summarises the average oxide layer thickness measured at RT and HT in both regions, CZ and FCZ. All specimens appear to exhibit comparable oxide thicknesses, with an average value of approximately 0.66 μm. In the contact zone, a reduction in oxide thickness would typically be expected due to surface friction, particularly at RT; however, this effect was not observed in the present measurements. This deviation may be attributed to the inherent variability in oxide growth across the surface. Previous research has reported that, after 6 h of exposure at 900 °C, the oxide layer in Inconel 718 reaches about 0.63 μm, increasing to 0.9 μm after 15 h [32], which aligns well with the values obtained in this study as a consequence of the applied heat treatment.

In conclusion, the existence of an oxide layer on the specimen surfaces is confirmed for both RT and HT conditions. Moreover, the thickness of this layer remains essentially consistent across all cases. These findings validate the authors' hypothesis that the oxide layer is formed during the thermal treatment process. Consequently, the reduction in fatigue life observed in high temperature tests is attributed to variations in the material's mechanical properties driven by temperature, rather than to the oxide layer developed during exposure [11–13].

5.2. Crack morphology

In plain fatigue tests conducted at RT, 83 % of the test specimens exhibited crack initiation at the corner, resulting in quarter-elliptical crack front. Conversely, in 17 % of the test specimens, cracks originated on the surface producing a semi-elliptical profile.

For the fretting fatigue tests at RT, all specimens developed through-thickness cracks, indicating that the crack propagated across the entire specimen thickness and advanced uniformly from the contact zone. Nevertheless, the initiation phase typically involved multiple semi-elliptical cracks that quickly merged into a single dominant through-thickness crack. One fatigue test, interrupted at a low maximum axial stress of 320 MPa after 1.13 million cycles, revealed the presence of a small semi-elliptical surface crack at the early stage of propagation.

For the fretting fatigue tests conducted at HT, two distinct crack initiation behaviours were identified, differentiated by variations in surface coloration. The first and most common behaviour involved multiple surface-initiated cracks that propagated in a semi-elliptical pattern before coalescing into a single through-thickness crack. In contrast, the second behaviour consisted of a single surface crack that progressively extended through the specimen until it extends through the entire specimen thickness, thereby forming a through-thickness crack. In most interrupted tests, several cracks were detected along the entire contact edge, further reinforcing the hypothesis that multiple crack initiations contribute to the eventual formation of a through-thickness crack.

5.3. Fretting scars

The scars caused by fretting on the contact zone are another crucial element to examine here, for that, two specimens were used in the present study to measure the contact scars: FF-RT(1)-8, which was tested at RT, and FF-HT(1)-11, which was tested at HT. Due to the fact that the contact surface is not homogeneous, the scar was measured using the occupied area, as Erena et al. [33], rather than directly measuring the scar. The acquired values were then compared to the theoretical semi-width of the contact as determined by Hertz's equation [34]:

$$a = \sqrt{\frac{8 \quad N R \quad (1 - \quad \nu^2)}{\pi E}} \tag{2}$$

To do this, the fretting scars were measured using an optical microscope in both contact zones developed by a single fretting bridge The experimental contact area was determined by means of microscopy (A_{exp}). With this value, an experimental value of the contact semi-width (a_{exp}) was calculated and compared with the theoretical Hertzian value (a_H).

The experimental contact semi-width was calculated by approximating the scar as a rectangular geometry with an average width. Therefore, the semi-width (a_{exp}) is calculated by dividing the measured scar area (A_{exp}) by the effective contact width (e_{eff}), and then dividing the result by two, as shown in the following equation:

$$2a_{\exp} = A_{\exp} / e_{eff} \tag{3}$$

Table 12
Comparison of experimental and Hertzian contact semi-widths in fractured and non-fractured zones.

	FF-RT(1)-8		FF-HT(1)-11	
	Fractured zone	**Non-fractured zone**	**Fractured zone**	**Non-fractured zone**
a_H (mm)	0.539	0.539	0.598	0.598
a_{exp} (mm)	0.609	0.550	0.622	0.602

This approach allows for a more accurate estimate of contact size when the surface is not perfectly uniform. The results reveal that the experimentally measured semi-width in the non-fractured area nearly matches the Hertzian prediction, while the fractured side has a higher semi-width than both the theoretical value and the non-fractured side.

For the RT specimen, the experimental measurements resulted in values of 0.609 mm in the fractured zone and 0.550 mm on the opposite side, compared with the theoretical value of 0.539 mm. In the case of the HT specimen, the measured semi-widths were 0.622 mm in the fractured zone and 0.602 mm on the opposite side, while the theoretical value was 0.598 mm. These results are summarised numerically in Table 12 and illustrated graphically in Fig. 17.

To quantify the effective contact width (e_{eff}), i.e. the fretted area (highlighted region), image analysis software NIS-Elements BR was employed. Once the region of interest was defined, the software

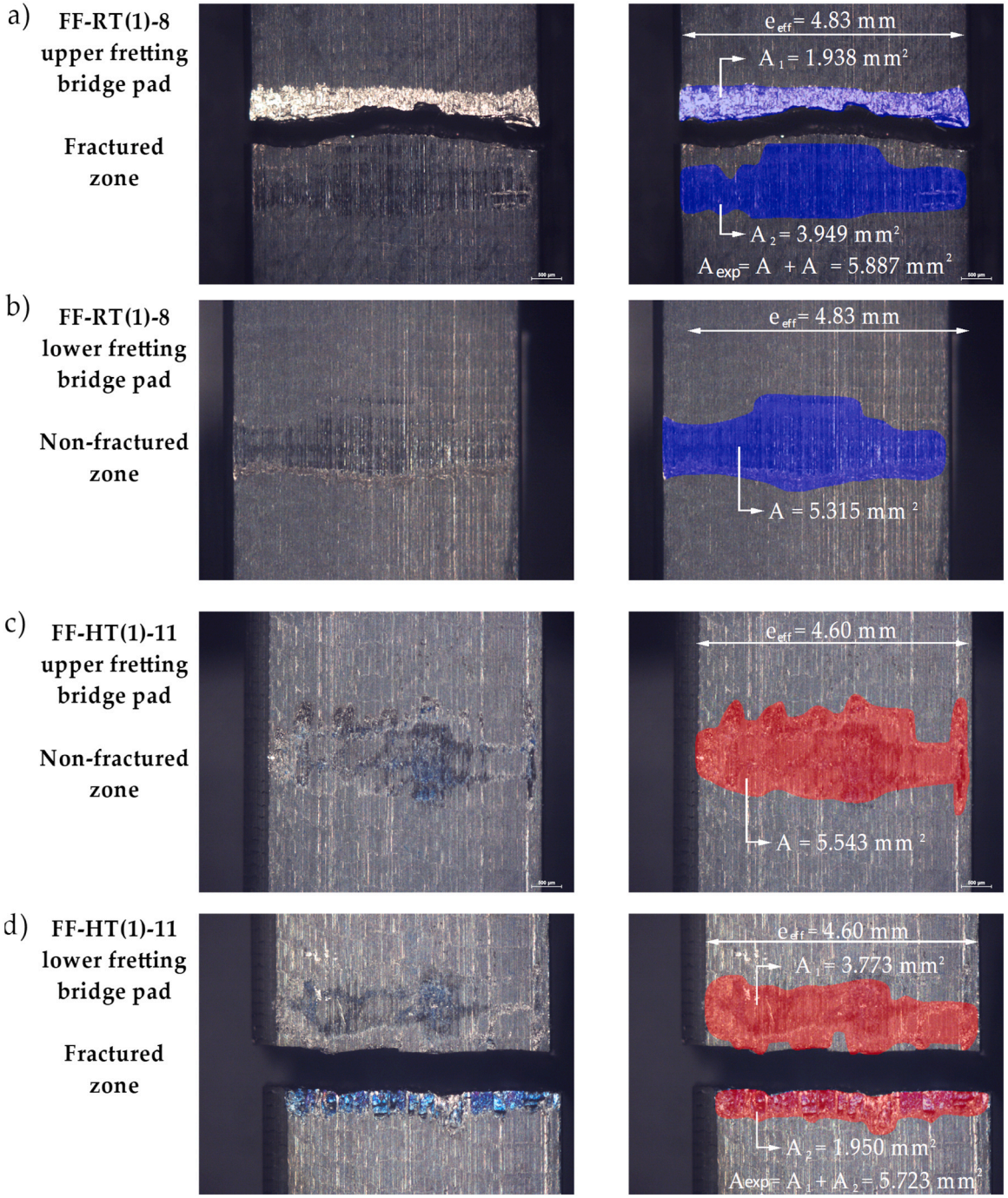

Fig. 17. Crack scar for two samples, one tested at RT and another at HT, FF-RT(1)-8 and FF-HT(1)-11 respectively.

automatically calculated the corresponding surface area.

These findings are similar with [33], who hypothesized that the increase in semi-width was caused by pad rotation throughout the test as well as stress redistribution in the fractured region. During fracture propagation, the stress distribution on the contact surface changes, which can result in localized scar expansion. Furthermore, accumulated plastic deformation and localized wear in this location may contribute to this phenomenon, resulting in a higher contact size than theoretical projections.

6. Conclusions

In this study, the effect of fretting fatigue on Inconel 718 with a conventional heat treatment was investigated at both room temperature and 650 °C. To achieve this, plain fatigue and fretting fatigue tests were conducted under various axial load levels, using an experimental procedure that had been previously validated in the laboratory.

The difference between fretting fatigue and plain fatigue was more noticeable at lower axial loads, and fretting fatigue led to shorter lifetimes at both temperatures. However, the fatigue lifetimes for plain and fretting situations were comparable at 1100 MPa, indicating that contact-induced stress concentration had no discernible impact at such stress levels.

With respect to the temperature effect, plain fatigue tests produced nearly identical results at both temperatures, though a slight reduction in life was observed at high temperature for specimens failing below 10^5 cycles. In contrast, fretting fatigue results tests at 650 °C showed lifetimes approximately four times shorter than those at room temperature in the entire life range tested, clearly demonstrating the influence of elevated temperature. Moreover, the difference between plain fatigue and fretting fatigue suggests that high temperature minimally impacts the crack initiation phase but significantly affects the crack propagation phase.

Additionally, the analysis of the normal load effect (7 and 10 kN) revealed that, within the range of conditions tested, the influence of normal load on fretting fatigue life was limited. The comparison between both loads showed similar trends for RT and HT, indicating that the change in normal load did not substantially modify the overall fatigue behaviour. Nonetheless, a slight improvement in the fatigue limit was observed at HT for the lower normal load of 7 kN.

Interrupted tests enabled the examination of crack morphology, showing that several semi-elliptical cracks initiated along the contact edge and quickly developed into through-thickness cracks. Introducing interruptions during testing appeared to slightly reduce the overall fatigue life, although the effect was not substantial. Furthermore, the number of interruptions did not appear to influence the final crack length.

SEM and EDS analyses confirmed the presence of oxide layers on the specimen surfaces, exhibiting comparable thicknesses at both room and high temperatures as a result of the applied heat treatment. Moreover, the oxygen content on the fracture surfaces was found to increase with longer exposure times at elevated temperature. Although oxidation was observed on the fracture surfaces, the present results do not establish a direct causal relationship between oxidation and the reduction of fretting fatigue life at high temperature. Regarding crack morphology, corner-initiated surface cracks predominated in plain fatigue tests at room temperature, whereas semi-elliptical surface cracks were more common under high-temperature conditions. In fretting fatigue tests, multiple semi-elliptical surface cracks developed along the contact edge and rapidly coalesced into through-thickness cracks.

CRediT authorship contribution statement

María Moreno-Rubio: Writing – original draft, Methodology, Investigation. **Jesús Vázquez:** Writing – review & editing, Supervision, Project administration, Methodology. **Carlos Navarro:** Writing – review & editing, Supervision, Project administration, Methodology. **Jaime Domínguez:** Supervision, Project administration.

Declaration of Competing Interest

The authors declare that they have no known competing financial interests or personal relationships that could have appeared to influence the work reported in this paper.

Acknowledgements

The authors wish to thank the Ministry of Science and Innovation for funding the research through the project RTI2018–096059-B-I00.

Data availability

Data will be made available on request.

References

[1] Golden PJ. Development of a dovetail fretting fatigue fixture for turbine engine materials. Int J Fatigue 2009;31(4):620–8.
[2] Ciavarella M, Demelio G. A review of analytical aspects of fretting fatigue, with extension to damage parameters, and application to dovetail joints. Int J Solids Struct 2001;38(s 10-13):1791–811.
[3] Erena D, Vázquez J, Navarro C, Domínguez J. Fatigue and fracture analysis of a seven-wire stainless steel strand under axial and bending loads. Fatigue Fract Eng Mater Struct 2020;43(1):149–61.
[4] Waterhouse R. Fretting fatigue. U.K: Applied science publischers; 1981.
[5] Waterhouse RB. Fretting at high temperatures. Tribology Int 1981:203–7.
[6] Abbasi F, Majzoobi G. An investigation into the effect of elevated temperatures on fretting fatigue response under cyclic normal contact loading. Theor Appl Fract Mech 2018;93:144–55.
[7] Sun Shouyi, Li Lei, He Kun, Yue Zhufeng, Yang Weizhu, Yu Zhiyuan. Fretting fatigue damage mechanism of Nickel-based single crystal superalloys at high temperature. Int J Mech Sci 2020;186.
[8] Zhang R, Meng X, Sun K, Li Q, Zhao F. An investigation of high and room temperature fretting fatigue of DD6-FGH96 dovetail joint in aero-engine: Experimental and numerical analysis. Int J Fatigue 2022;154.
[9] R.M.N. Fleury, Investigation of fretting fatigue in turbine fir tree blade to disc joints at high temperature [Ph.D. thesis], University of Oxford, 2015.
[10] Fang J, Han Q, Cui H, Lei X, Yan X, Mu Q. Fretting fatigue experiment and polycrystal plasticity simulation in Ni-based superalloy at room temperature and 650°C. Int J Fatigue 2023;168(107460).
[11] Mall S, Kim H-K, Porter WJ, Ownby JF, Traylor AG. High temperature fretting fatigue behavior of IN100. Int J Fatigue 2010;32(8):1289–98.
[12] Kwon J-d, Park D-k, Woo S-w, Yoon D-h, Chung I. A study on fretting fatigue life for the Inconel alloy 600 at high temperature. Nucl Eng Des 2010;240:2521–7.
[13] Kwon J-d, Jeung H-k, Chung I, Yoon D-h, Park D-k. A study on fretting fatigue characteristics of Inconel 690 at high temperature. Tribology Int 2011;44:1483–7.
[14] Almeida G, Cardoso R, Chassaing G, Pommier S, Araújo J. Fretting fatigue of Inconel 718 at room and elevated temperatures considering both constant and cyclic normal contact loads. Tribology Int 2023;183(108382).
[15] Wang J, Huang Z, Jia Z, Bian M, Yang Z, He H. Investigation on fretting fatigue crack initiation of IN718 alloy in very high cycle regime. WEAR 2025;572.
[16] Moreno-Rubio M, Vázquez J, Navarro C, Domínguez J. Experimental study on the fretting fatigue of Inconel 718 superalloy. Tribology Int 2023;186(108637).
[17] I. Diego, Analysis of relevant factors affecting fretting fatigue behaviour of aeronautical alloys, Universidad Carlos III de Madrid, 2020.
[18] Kattoura Micheal, Mannava Seetha Ramaiah, Quian Dong, Vasudevan Vijay K. Effect of laser shock peening on elevated temperature residual stress, microstructure and fatigue behavior of ATI 718Plus alloy. Int J Fatigue 2017;104:366–78.
[19] C. Navarro, Iniciación y Crecimiento de Grietas en Fatiga por Fretting, *Tesis Doctoral. Universidad de Sevilla,* 2005.
[20] O. Dugauguez, Application of unconventional methods to MIM Inconel 718 components [Ph.D. Thesis], Universidad Carlos III de Madrid, 2017.
[21] Caliari F, Candioto K, Reis D, Couto A, Neto C, Nunes C. Study of the mechanical behavior of an inconel 718 aged superalloy submitted to hot tensile tests. SAE Tech Pap 2011;36(0328).
[22] Sonar Tushar, Balasubramanian Visvalingam, Malarvizhi Sudersanan, Venkateswaran Thiruvenkatam, Sivakumar Dhenuvakonda. An overview on welding of Inconel 718 alloy - Effect of welding processes on microstructural evolution and mechanical properties of joints. Mater Charact 2021;174(110997).
[23] Sugahara T, Augusto C A, Ribeiro B MJ, Piorino N F, Takahashi RJ, Pereira R DA. Creep and mechanical behavior study of inconel 718 superalloy. Mater Res 2022;25.
[24] JSME Standard method of fretting fatigue testing, JSME S 015-2002, The Japan Society of Mechanical Enineers, 2002.

[25] Kuliiev R, Riekehr S, Ventzke V, Keller S, Kashaev N. On the effect of testing frequency on high and very high cycle fatigue behavior of AA2024-T3, Ti-6Al-4V, and Inconel 718. J Mater Eng Perform 2023;32(23):10843–56.
[26] Navarro C, Dominguez J. Initiation criteria in fretting fatigue with spherical contact. Sci Direct 2004;26:1253–62.
[27] Wittkowsky BU, Birch PR, Dominguez J, Suresh S. An apparatus for quantitative fretting fatigue testing. Fatigue FRact Engng Mater Struct 1998;22:307–20.
[28] Navarro C, Vázquez J, Domínguez J. A general model to estimate life in notches and fretting fatigue. Eng Frct Mech 2011;78(8):1590–601.
[29] Kawagoishi N, Chen Q, Nisitani H. Fatigue strength of Inconel 718 at elevated temperatures. Fatigue Fract Eng Mater Struct 2000;23:209–16.
[30] Maurizio DAPOR. Penetration of an electron beam in a solid material: a simple model and a numerical simulation. Phys Lett a 1990;143(3).
[31] Gajapathi Satya S, Mitra Sushanta K, Mendez Patricio F. Controlling heat transfer in micro electron beam welding using volumetric heating. Int J Heat Mass Transf 2011;54(25-26):5545–53.
[32] Delaunay F, Berthier C, Lenglet M, Lameille J. SEM-EDS and XPS studies of the high temperature oxidation behaviour of inconel 718. Mikrochim Acta 2000;132: 337–43.
[33] Erena D, Martín V, Vázquez J, Navarro C. Influence of the rolling of contact pads on crack initiation in fretting fatigue test. Int J Fatigue 2022;163(107087).
[34] Hills DA, Nowell D. Mechanics of fretting fatigue. Springer; 1994.